Intra-annual variations of spectrally resolved gravity wave activity in the UMLT region

René Sedlak[1], Alexandra Zuhr[1,2,a], Carsten Schmidt[2], Sabine Wüst[2], Michael Bittner[1,2], Goderdzi G. Didebulidze[3], Colin Price[4]

[1]Institute of Physics, University of Augsburg, Augsburg, Germany
[2]German Remote Sensing Data Center, German Aerospace Center, Oberpfaffenhofen, Germany
[3]Georgian National Astrophysical Observatory, Ilia State University, Tbilisi, Georgia
[4]Porter School of the Environment and Earth Sciences, Tel Aviv University, Israel
[a]now at: Alfred Wegener Institute, Helmholtz Center for Polar and Marine Research, Bremerhaven, Germany

Correspondence to: René Sedlak (rene.sedlak@physik.uni-augsburg.de)

Abstract. The period range between 6 min and 480 min is known to represent the major part of the gravity wave spectrum driving mesospheric dynamics. We present a method using wavelet analysis to calculate gravity wave activity with a high period-resolution and apply it to temperature data acquired with the OH* airglow spectrometers GRIPS (GRound-based Infrared P-branch Spectrometer) within the framework of the NDMC (Network for the Detection of Mesospheric Change; https://ndmc.dlr.de). We analyse data measured at the NDMC sites Abastumani in Georgia (ABA, 41.75° N, 42.82° E), ALOMAR in Norway (ALR, 69.28° N, 16.01° E), Neumayer III in the Antarctic (NEU, 70.67° S, 8.27° W), Observatoire de Haute-Provence in France (OHP, 43.93° N, 5.71° E), Oberpfaffenhofen in Germany (OPN, 48.09° N, 11.28° E), Sonnblick in Austria (SBO, 47.05° N, 12.95° E), Tel Aviv in Israel (TAV, 32.11° N, 34.80° E), and the Environmental Research Station Schneefernerhaus on top of Mt. Zugspitze, Germany (UFS, 47.42° N, 10.98° E). All eight instruments are identical in construction and deliver consistent and comparable data sets.

For periods shorter than 60 min, gravity wave activity is found to be relatively low and hardly shows any seasonal variability on the time scale of months. We find a semi-annual cycle with maxima during winter and summer for gravity waves with periods longer than 60 min, which gradually develops into an annual cycle with a winter maximum for longer periods. The transition from a semi-annual pattern to a primarily annual pattern occurs around a gravity wave period of 200 min. Although there are indications of enhanced gravity wave sources above mountainous terrain, the overall pattern of gravity wave activity does not differ significantly for the abovementioned observation sites. Thus, large-scale mechanisms such as stratospheric wind filtering seem to dominate the temporal course of mesospheric gravity wave activity.

Atmospheric
Measurement
Techniques
Discussions
EGU
Open Access

1 Introduction

Gravity waves represent an important coupling mechanism between different atmospheric regions by transporting energy and momentum not only horizontally but also vertically. While they are often generated in the lower atmosphere, their influence can even reach up to the ionosphere (Laštovička, 2006). It is widely accepted that gravity waves significantly

5 determine global circulation patterns, most prominently the mean residual meridional circulation (Holton, 1983; Garcia & Solomon, 1985). They interact with large-scale dynamical structures such as planetary waves and are able to accelerate or decelerate atmospheric jets by momentum deposition (Hines, 1960; Hodges, 1969; Lindzen, 1981).

In order to take adequate account of their influence on global atmospheric dynamics – especially in view of predicting the effects of climate change – detailed knowledge of gravity wave parameters such as the amount of transported energy is

10 essential. Especially in the UMLT (upper mesosphere / lower thermosphere) – the hot-spot region of gravity wave drag release (Gardner et al., 2002) – in situ measurements are hardly possible. Nevertheless, a variety of remote sensing techniques measuring at different locations allow the derivation of the potential energy density (Rauthe et al., 2008; Wüst et al., 2016, 2017a) or of the ambiguous gravity wave activity parameter (Gavrilov et al., 2004; Hibbins et al., 2007; Beldon & Mitchell, 2009; Offermann et al., 2009; Hoffmann et al., 2010, please note that the term 'gravity wave activity' does not

15 have the same meaning in all these publications – it refers either to variations of wind or temperature caused by gravity waves) for different parts of the gravity wave spectrum. However, the results do not always agree concerning the intra-annual variability. This could be due to the different geographical positions of the observations and/or to the different data reduction and analysis algorithms and/or to the differing spectral ranges to which the instruments are sensitive (observational filter). Wüst et al. (2016, 2017a) showed that the spectral range is of importance in this context. The authors applied identical

20 data reduction and analysis algorithms to temperature time series of identical OH* spectrometers and found that the gravity wave potential energy density (GWPED) evolves differently during the year for periods longer and shorter than 60 min.

We have analysed gravity wave activity based on data of eight infrared spectrometers called GRIPS (GRound-based Infrared P-branch Spectrometer) that are identical in construction and operated at different locations worldwide within the Network

25 for the Detection of Mesospheric Change (NDMC, https://ndmc.dlr.de). The brightest component of the nocturnal airglow is created by excited hydroxyl molecules (OH*) in the UMLT emitting radiation in the visible and in the near infrared wavelength spectrum (Meinel, 1950; Leinert et al., 1998). The peak emission height of the OH* layer is located at about 87 km height on average (Baker & Stair, 1988; von Savigny et al., 2004; Melo et al., 2000; Wüst et al., 2017b). As gravity waves are causing local temperature fluctuations, they are modulating the emission behaviour of the OH* molecules (see for

30 example Svenson & Gardner, 1998). This makes gravity waves and other dynamical features visible in the images of infrared cameras (see e.g. Taylor, 1997; Pautet et al., 2014; Hannawald et al., 2016; Sedlak et al., 2016; Hannawald et al., 2019; Wüst et al., 2019) but also in the time series of OH* rotational temperatures (Hines & Tarasick, 1987; Simkhada et al., 2009; Reisin & Scheer, 2001; Offermann et al., 2009; Wachter et al., 2015; Wüst et al., 2016, 2017a, 2018; Silber et al., 2017).

These are found to be in good agreement with the kinetic mesospheric temperatures (see e.g. Bittner et al., 2010; Noll et al., 2016) and can be derived from the line intensities of the OH* airglow radiation, which are measured with spectrometers (Mulligan et al., 1995; Espy & Stegman, 2002; Espy et al., 2003; French & Burns, 2004; Schmidt et al., 2013, 2018).

5   In this work, we make use of wavelet analysis, which allows us to derive spectrally-resolved gravity wave activity from time series of OH* rotational temperatures. In this way, we address gravity waves with periods in a comparatively broad range of $6-480\,\mathrm{min}$ separately. Such a climatology resolving the spectrum of gravity waves is not available yet. The scientific focus of this paper is to reveal the period-dependence of the intra-annual cycles of gravity wave activity in the UMLT.

In section 2, the data sets we used are presented together with a description of the quality criteria we have applied. In section
10   3, we introduce the analysis and show the intra-annual cycles of period-resolved gravity wave activity. They are discussed in section 4 and the main results are summarized in section 5.

2 Data basis

GRound-based Infrared P-branch Spectrometers (GRIPS) are sensitive to electro-magnetic radiation in the near infrared. The intensities of the $P_1(2)$, $P_1(3)$, and $P_1(4)$ rotational lines of the OH(3-1) vibrational transition at 1.524, 1.534 and 1.543 µm are used to derive the rotational temperatures of the OH* airglow layer. This is done by assuming local thermodynamic

5 equilibrium in the mesopause region (Noll et al., 2019). Due to solar radiation, measurements are only possible during the night-time.

GRIPS instruments are equipped with a 512 pixels InGaAs-photodiode array, which has its maximum sensitivity between 1.5 and 1.6 µm. The temporal resolution ranges from 5 to 15 s. Further technical details can be found in Schmidt et al. (2013).

10 Measurements were started in 2009, when GRIPS 6 was put into operation at the DLR site Oberpfaffenhofen (OPN, 48.09° N, 11.28° E), Germany. The number of GRIPS instruments has increased since then. Today, fourteen instruments (GRIPS 5 to 18) are operated within the Network for the Detection of Mesospheric Change (NDMC, https://ndmc.dlr.de) providing extensive coverage around the globe. In this work, temperature series of eight different GRIPS instruments are used. Besides the GRIPS 6 time series, we analysed data acquired by GRIPS 8 at the Environmental Research Station Schneefernerhaus

15 (UFS, 47.42° N, 10.98° E) below the summit of Mt Zugspitze in Germany, by GRIPS 16 at the Sonnblick Observatory (SBO, 47.05° N, 12.95° E) in Austria and by GRIPS 12 at the Observatoire de Haute-Provence (OHP, 43.93° N, 5.71° E) in France. The measurements above the Alps and their foothills are compared to data from the Lesser Caucasus (GRIPS 5 at the Abastumani Astrophysical Observatory, ABA, 41.75° N, 42.82° E in Georgia) and the Mediterranean (GRIPS 10 at Tel Aviv, TAV, 32.11° N, 34.80° E in Israel). Apart from that, we also analyse data from polar regions. GRIPS 9 was deployed

20 at the Arctic Lidar Observatory for Middle Atmosphere Research, ALOMAR (ALR, 69.28° N, 16.01° E), Norway during a measurement campaign from winter 2010/11 to spring 2014. Measurements with GRIPS 15 are performed at the Neumayer-Station III (NEU, 70.67° S, 8.27° W) in the Antarctic since March 2013. The start and end dates of the times series analysed in this publication are shown in Table 1 for each observation site.

As the temporal resolution of the GRIPS instruments is much better than necessary for retrieving gravity waves, the data sets

25 are averaged to one-minute means in order to reduce noise. Before calculating the gravity wave activity from these time series, the data need to satisfy several criteria concerning data quality, data gaps and length of the data series. The data quality criteria agree with the ones presented in Wüst et al. (2016, 2017a): only temperature values which have an uncertainty of less than or equal to 4.5 K and have been measured during episodes of a solar zenith angle larger than 100° (in order to avoid artefacts due to enhanced solar radiation during sunset or sunrise) are considered. Nocturnal temperature

30 series are further analysed, if they consist of at least 240 succeeding values (corresponding to a time period of four hours). If more than one of such episodes is available for one night, we used only the longest one for further analysis.

In contrast to Wüst et al. (2016), who used an iterative approach of sliding means to calculate potential energy density, a wavelet analysis will be used in this work. This analysis method requires an equidistant time series. However, bad weather

(clouds) frequently causes data gaps. They are extrapolated based on the ten preceding data points by the maximum entropy method (MEM; see e.g. Ulrych and Bishop, 1975) in its capacity as a linear prediction filter (Bittner et al., 2000, Höppner & Bittner, 2007), if the data gaps are not larger than six minutes.

Due to meteorological and geophysical reasons, the monthly data coverage varies (Figure 1). For high-latitudinal stations
5   (NEU, ALR), it suffers from midnight sun during polar summer. Also Alpine stations (SBO, UFS) show a minimum of observations during summer. However, in these cases this effect is mainly due to bad weather. The station at TAV exhibits a rather inhomogeneous data distribution due to stray light and technical issues (Wüst et al., 2017a).

Table 1. Start and end dates of the analysed time series for the respective station. The same start dates as in Wüst et al. (2016,
10 2017a) have been chosen for each data set as far as the respective stations have been analysed therein.

Station	Instrument	Start of analysed time series	End of analysed time series	Total number of nights	Number of nights observed	Number of nights analysed
ABA (41.75° N, 42.82° E)	GRIPS 5	2012/10/15	2018/06/05	2001	1974	853
ALR (69.28° N, 16.01° E)	GRIPS 9	2011/01/01	2014/04/08	1192	875	277
NEU (70.67° S, 8.27° W)	GRIPS 15	2013/03/18	2018/06/01	1900	1402	394
OHP (43.93° N, 5.71° E)	GRIPS 12	2012/06/28	2018/06/01	2164	2152	882
OPN (48.09° N, 11.28° E)	GRIPS 6	2011/01/08	2018/06/05	2704	2622	708
SBO (47.05° N, 12.95° E)	GRIPS 16	2015/08/05	2018/05/12	1011	1006	235
TAV (32.11° N, 34.80° E)	GRIPS 10	2011/11/25	2016/01/26	1523	1478	249
UFS (47.42° N, 10.98° E)	GRIPS 8	2011/01/05	2018/06/02	2704	2646	835

Atmospheric
Measurement
Techniques
Discussions

3 Analysis and results

The wavelet analysis is a time-dependent spectral analysis method. In contrast to other analyses, e.g. the harmonic analysis, which assumes stationary periodic signatures (Bittner et al., 1994), the wavelet analysis can identify transient wave signals, which makes it well suited for the identification of gravity wave signatures. A comprehensive mathematical description of the wavelet analysis can be found in Chui (1992). We use the wavelet analysis as it was described by Ochadlick et al. (1993) based on a Morlet wavelet and apply it to the temperature time series of each night. The wavelet analysis then delivers a two-dimensional wave spectrum that depends on time and period (resolution of 1 min in both domains).

In order to perform a significance test, the wavelet analysis is repeated another eleven times for randomly generated data (white noise), which have been provided with the same statistical properties (i.e. mean value and standard deviation) and length as the original temperature series (see also Höppner and Bittner, 2007). For every period, the 99 % quantile of the wavelet intensities in the random spectra is considered as the level of significance. For a time series of 100 min, for example, this means that the 99% quantile is calculated based on 1100 values for every period.

The mean nocturnal value of the gravity wave activity in the period range $[\tau_1; \tau_2]$ is retrieved by calculating the averaged significant wavelet intensity between τ_1 and τ_2 throughout the analyzed night length. The spectra are altered by randomly varying each temperature value within its error bar (4.5 K at maximum). The mean deviation of ten altered spectra from the original spectrum is taken as a measure of the uncertainty for the mean nocturnal value. In the further course of this publication we calculate monthly mean values. Here we use the standard error of the mean ($\sigma/\sqrt{N}$; with σ being the standard deviation and N the number of values), which is larger than the uncertainty resulting from the individual error bars.

The short-periodic limit of gravity waves is defined by the Brunt-Väisälä frequency, which ranges between 4 and 5 min in the UMLT (Wüst et al., 2017b). We restrict our analysis to periods of at least 6 min. The upper limit of 240 min (4 h), which we chose for gravity wave periods in the first run, is the minimum length of the analyzed nocturnal temperature series. This upper limit is raised to 480 min (8 h) in a second analysis. The influence of tides can be tentatively neglected as we limit our analyses to periods below 8 h. Apart from that, Offermann et al. (2009) note on basis of the Global Scale Wave Model (GSWM) in combination with a climatology based on satellite data of TIMED-SABER (Thermosphere Ionosphere Mesosphere Energetics Dynamics, Sounding of the Atmosphere using Broadband Emission Radiometry) that the tidal influence is small compared to gravity wave signatures at extratropical latitudes.

The examination of the response behaviour of the wavelet analysis using synthetic test data sets revealed that oscillations with shorter periods yield slightly higher peak intensities in the wavelet spectrum than oscillations with longer periods having the same amplitude. Our tests have shown that the peak wavelet intensity decays linearly for increasing periods. Furthermore, the response peak is blurred over a wider range of periods for longer periodicities. This makes it difficult to link absolute values of wavelet intensity to actual temperature amplitudes of the respective oscillations. However, in this work we focus on the relative behaviour of period-resolved wave activity. Additional calculations (not shown here) have

Atmospheric
Measurement
Techniques
Discussions

Open Access

EGU

shown that the period-dependence of the wavelet response is small enough not to affect the resulting behaviour of gravity wave activity.

Figure 2 shows the nocturnal mean of the significant wavelet intensity averaged over each month for the period range $\tau \in [6\,\text{min}; 480\,\text{min}]$ with $\Delta\tau = 1\,\text{min}$ for each station. The average behaviour at the different observation sites is quite

5   similar. The mean wavelet intensity is close to zero for periods shorter than 25 min and starts increasing for longer periods. While there is hardly any variability on monthly scales for gravity waves with periods below 60 min, a semi-annual cycle emerges for periods longer than 60 min, which is characterized by maximum values in winter and summer. This semi-annual cycle gradually turns into an annual cycle with a strong maximum during winter and minimum values during summer for gravity wave periods longer than ca. 200 min (230 min in the case of SBO, 160 min in the case of ABA). This spectrally

10   dependent evolution of the intra-annual shape of gravity wave activity can be well recognized when averaging the monthly values over all years. This is demonstrated in Figure 3 using the data of OPN.

The standard deviation of the monthly mean values of significant wavelet intensity can be calculated for each period (see Figure 4). As Figure 2 already suggests, the standard deviation of the monthly mean gravity wave activity is mostly increasing for larger periods. Similar to the mean value of wavelet intensity the standard deviation begins to increase

15   remarkably at a period of 25 min. For periods longer than 60 min, the curves start separating from one another rather than following a common course. This supports the approach of analysing gravity waves with periods shorter and longer than 60 min separately as Wüst et al. (2016, 2017a) did. It is interesting to note the occurrence of local peaks in the standard deviation graphs (Figure 4). A local peak of enhanced variability can be found at a period around 45 min for six out of eight stations (ABA, ALR, NEU, OHP, SBO, TAV). Another peak, or at least a strongly increased slope, is visible around a period

20   of 105 min for four out of eight stations (ABA, SBO, TAV, UFS). Other local peaks can be found at periods of about 80 min (NEU, UFS, TAV; shoulder at ALR and SBO) and about 160 min (SBO and TAV).

4 Discussion

Wüst et al. (2016, 2017a) calculated the GWPED for the same measurement nights acquired at OPN, UFS, ALR, OHP and TAV as we did. The authors applied a combination of different sliding mean filters to the temperature time series and distinguished between the short-period (shorter than 60 min) and long-period (longer than 60 min) wave range. In order to

5   compare our results to the ones of those authors, we calculated the nocturnal mean values of wavelet intensity in the period ranges 6–60 min, 60–240 min and 60–480 min and averaged the monthly mean values over all years for all stations (Figure 5). For the stations with data coverage throughout the entire year, the wavelet intensity averaged for periods 6–60 min shows very low seasonal variation with a weak summer maximum in some cases, whereas a semi-annual oscillation with maxima during winter and summer is visible when averaging wavelet intensity in the period range 60–240 min. This can even be

10   observed for TAV despite the seasonally inhomogeneous data coverage. A dominant annual course with a winter maximum can be recognized for ABA, OHP, OPN and UFS when averaging the wavelet intensity between periods of 60 and 480 min. For SBO and TAV this statement is difficult to confirm within the given error bars. As concerns the polar stations ALR and NEU, wavelet intensity in the period ranges 60–240 min and 60–480 min is higher during the winter months of the respective hemisphere than in spring and autumn. Due to the missing data during polar summer there is no information about

15   a secondary summer maximum.

In contrast to Wüst et al. (2016, 2017a), we need nearly undisturbed time series of 240 min (nearly undisturbed means that we interpolate data gaps of up to 6 min) for our analysis and the wavelet method is only applied to the longest of such episodes of a night (see section 2). Especially during winter when the weather is cloudy, this leads to differences in the data bases used by Wüst et al. (2016, 2017a) and us. Our data basis is smaller. However, a systematic influence of the differing

20   data bases could be excluded by applying the GWPED algorithm of Wüst et al. (2016, 2017a) to our smaller data basis: the observed seasonal cycles remained persistent (not shown).

Hence, our findings agree well with the results of Wüst et al. (2016, 2017a) who hardly find any seasonal variability of short-period GWPED and a dominant annual cycle with a maximum during winter in the long-period case. Even minor features like their secondary peak in May at OHP are similar to our cycles of long-periodic GWPED.

25   There are a number of further publications supporting both, the observation of an annual and of a semi-annual oscillation of gravity wave activity. Rauthe et al. (2008) discovered an annual cycle with winter maxima in temperature variations between 35 and 90 km height when analyzing intervals of 3–5 h at mid-latitudes. The year before Hibbins et al. (2007) published wind variations derived from radar data, which also exhibit an annual variation with a winter maximum in the altitude range 74–94 km above Rothera, Antarctica. They analysed the spectral range between 4 min and 8 h. Beldon & Mitchell (2009)

30   point out that the annual mode may tend to be found in the mid- to low-frequency range of the gravity wave spectrum. Also above Rothera, Antarctica they found a semi-annual oscillation with a second maximum during summer after having restricted their analysis to oscillations shorter than 200 min, which fits quite well with our results. The authors consider the polar night jet as a possible reason for the annual component. Offermann et al. (2009) extracted gravity wave activity by

Atmospheric
Measurement
Techniques
Discussions

calculating the standard deviation of mesopause temperatures, which also shows a semi-annual behavior with a primary summer maximum and a secondary but still strong winter maximum. Gavrilov et al. (2004) found a semi-annual behavior of wind variances between 10 min and 5 h below 82 – 85 km altitude above Hawaii. Hoffmann et al. (2010) presented an annual variation with a secondary summer maximum in wind variances between 3 and 9 h at Andenes, Norway and Juliusruh,

5   Germany, which is enhanced when only looking at periods below 2 h. They conclude from their own and from preceding work that the summer maximum of gravity wave activity seems to be dominated by waves with periods smaller than 6 h.

All these authors agree in finding enhanced gravity wave activity during winter. This could be attributed to wind filtering. During winter, the vertical profile of the zonal wind is purely eastward so that nearly all eastward-travelling gravity waves

10   encounter critical levels in the strong westerlies and are filtered. The entire spectrum of westward propagating gravity waves however can ascend into the UMLT without encountering filtering by the zonal background wind. The stratospheric jet is reversed to westward direction during summer, filtering out most of the westward-oriented spectrum of gravity waves. Additionally, large parts of the eastward-propagating spectrum are filtered by the tropospheric jet unless the phase velocity is high enough. This implies a higher gravity wave activity during winter compared to summer if tropospheric gravity wave

15   sources are considered.

The fact that in our investigations summer gravity wave activity for periods between 60 and 240 min is roughly as high as winter-time activity may point to a significant contribution of gravity wave sources at altitudes above the stratospheric wind fields. Due to strong temperature and wind field changes the UMLT region itself can also act as a source of gravity waves, especially in the short-periodic range (see e.g. Didebulidze et al., 2004). While the mean emission height of the OH airglow

20   layer stays more or less constant throughout the year (Wüst et al., 2017b), lidar measurements have shown that the mesopause is located at about 86 km in summer and rises to about 100 km altitude during winter (Lübken and von Zahn, 1991; She et al., 1993). This provides the possibility for observed waves to grow to larger amplitudes in summer. Apart from this, seasonally varying sources for gravity waves like extratropical storm systems, which are more apparent during winter, may also contribute to enhanced gravity wave activity even in the UMLT (e.g. Kramer et al., 2015, 2016 and references

25   therein).

Minimum gravity wave activity at the equinoxes could possibly be attributed to stratospheric wind reversal. During these episodes both eastward and westward travelling gravity waves with low phase speeds encounter critical level filtering (Hoffmann et al., 2010). Assuming a Gaussian-shaped distribution of gravity wave phase speeds centered around zero it follows that most of the waves are filtered (Beldon & Mitchell, 2009). Based on these assumptions it would not be surprising

30   that wind filtering of this central part of the gravity wave spectrum during the equinoxes leads to minimum wave activity in the UMLT region. However, it has to be noted that these are theoretical considerations which cannot be proven by our measurements alone.

In the spectrally resolved distribution of standard deviation of the wavelet intensity several local peaks were identified, most prominently around 45 min, 80 min, 105 min, and 160 min, which occur for more than one station. The peaks are in particular present for the data sets of OHP and UFS – the stations with the longest and best data coverage. These might be periods at which gravity waves are particularly sensitive to wind filtering (their phase velocity varies around the stratospheric wind

5 maximum assuming a tropospheric source, for example) or these periods are generated only from time to time (due to convective sources, for example).

As concerns the direct comparison between the different observation sites, which are mostly situated in or near mountainous regions, there are hardly any systematic differences in the intra annual cycle even though the instruments are deployed at

10 different parts of Europe. This agrees with the concept that although being a rather small-scale dynamical feature itself, the overall activity of gravity waves in the UMLT is mainly shaped by large-scale mechanisms, most prominently wind filtering. However, there are some minor local deviations. As one may deduce from Figure 5 at ABA the increase of the mean wavelet intensity from periods $60-240$ min to periods $60-480$ min in most months is a bit higher than for the other mid-latitude stations. This might be attributed to regional peculiarities in the Caucasus.

15

Atmospheric
Measurement
Techniques
Discussions

5 Summary and outlook

We apply a combination of MEM and wavelet analysis in order to calculate gravity wave activity with a high spectral resolution from UMLT temperature time series. The data we analysed have been acquired with identically built spectrometers called GRIPS at the DLR site Oberpfaffenhofen (OPN), Germany, the Environmental Research Station

5   Schneefernerhaus (UFS) on Mt. Zugspitze, Germany, Sonnblick Observatory (SBO), Austria, Observatoire de Haute-Provence (OHP), France, Abastumani Astrophysical Observatory, (ABA), Georgia, Tel Aviv (TAV), Israel, the Arctic Lidar Observatory for Middle Atmosphere Research ALOMAR (ALR), Norway, and at Neumayer-Station III (NEU) in the Antarctic. Most stations are situated at or near mountainous regions.

The intra-annual behaviour of gravity wave activity in the UMLT region turns out to be strongly dependent on the wave

10   period. At nearly all stations that allow all-season observations we find a clear semi-annual pattern of gravity wave activity for periods longer than 60 min with maximum activity during winter and summer and minimum activity during spring and autumn. The semi-annual cycle turns into an annual cycle with a winter maximum and a summer minimum for longer periods. Our investigations reveal that the transition from semi-annual to annual behaviour occurs around a period of 200 min. There is hardly any seasonal variation for periods shorter than 60 min.

15   Although the different instruments are deployed at quite different locations (in the Alpine region, in the Lesser Caucasus, in the Antarctic, near the Scandinavian and Israel coastal plain), the overall findings agree very well. This suggests a general or global reason for the observed intra annual variations such as wind filtering. It can explain the observed annual and semi-annual modes of gravity wave activity in the UMLT under the following assumptions: gravity waves with periods between 60 and 240 min (240 min and 480 min) are generated at altitudes of or above (below) the stratospheric jet.

20   Local variations are visible in the variability of gravity wave periods: there exist gravity wave periods which vary more in activity with time than others.

The algorithm presented here has been applied operationally to observations since June 2018. If the GRIPS data of a measurement night are of sufficient quality (see section 2), they are automatically processed during the following night. The data products are being integrated into the NDMC at the moment, so that information about the current gravity wave activity

25   will soon be provided at https://ndmc.dlr.de for all active GRIPS stations. The spectrally resolved proxy of gravity wave activity at the Alpine stations will also be included into the Alpine Environmental Data Analysis Center (AlpEnDAC, https://www.alpendac.eu) in order to complement Alpine climate research within the scope of the Virtual Alpine Observatory (VAO, https://www.vao.bayern.de).

6 Data availability

30

The data are archived at the WDC-RSAT (World Data Center for Remote Sensing of the Atmosphere). The GRIPS instruments are part of the Network for the Detection of Mesospheric Change, NDMC (https://ndmc.dlr.de).

Atmospheric
Measurement
Techniques
Discussions

EGU

Author contribution

The conceptualisation of the project, the funding acquisition as well as the administration and supervision was done by MB
5 and SW. The operability of the instrument was assured by CS. GD and CP took care of the maintenance at ABA and TAV, respectively. The algorithm was written and tested by AZ and RS. The data analysis and visualization was done by RS. The interpretation of the results benefited from discussions between SW, MB, CS, and RS. The original draft of the manuscript was written by RS. Careful review of the draft was performed by all co-authors.

Competing interests

10 The authors declare that they have no conflict of interest.

Atmospheric
Measurement
Techniques
Discussions

References

Baker, D. J. and Stair, A. T.: Rocket Measurements of the Altitude Distributions of the Hydroxyl Airglow, Phys. Scripta, 37, 611–622, 1988.

Beldon, C. L., and Mitchell, N. J.: Gravity waves in the mesopause region observed by meteor radar, 2: Climatologies of gravity waves in the Antarctic and Arctic, J. Atmos. Sol.-Terr. Phy., 71, pp. 875-884, 2009.

Bittner, M., Offermann, D., Bugaeva, I. V., Kokin, G. A., Koshelkov, J. P., Krivolutsky, A., Tarasenko, D. A., Gil-Ojeda, M., Hauchecorne, A., Lübken, F.-J., de la Morena, B. A., Mourier, A., Nakane, H., Oyama, K. I., Schmidlin, F. J., Soule, I., Thomas, L., and Tsuda, T.: Long period/large scale oscillations of temperature during the DYANA campaign, J. Atmos. Terr. Phys., Vol. 56, Nos. 13/14, pp. 1675-1700, 1994.

Bittner, M., Offermann, D., and Graef, H. H.: Mesopause temperature variability above a midlatitude station in Europe, J. Geophys. Res., Vol. 105, No. D2, pp. 2045-2058, 2000.

Bittner, M., Höppner, K., Pilger, C., and Schmidt, C.:Mesopause temperature perturbations caused by infrasonic waves as a potential indicator for the detection of tsunamis and other geo-hazards, Nat. Hazards Earth Syst. Sci., 10, 1431-1442, 2010.

Chui, C. K.: An Introduction to Wavelets, Wavelet Analysis and its Applications, Vol. 1, 1992.

Didebulidze, G. G., Kafkalidis, J. F., and Pataraya, A. D.: Coupling processes between atmospheric vertical perturbations and acoustic-gravity waves in the mesosphere-thermosphere regions, J. Atmos. Sol.-Terr. Phys., 66, pp. 715-732, 2004.

Espy, P. J., and Stegman, J.: Trends and variability of mesospheric temperature at high-latitudes, Phys. Chem. Earth, 27, pp. 543-553, 2002.

Espy, P. J., Hibbins, R. E., Jones, G. O. L., Riggin, D. M., and Fritts, D. C.: Rapid, large-scale temperature changes in the polar mesosphere and their relationship to meridional flows, Geophys. Res. Letters, Vol. 30, No. 5, 1240, doi:10.1029/2002GL016452, 2003.

French, W. J. R., and Burns, G. B.: The influence of large-scale oscillations on long-term trend assessment in hydroxyl temperatures over Davis, Antarctica, J. Atmos. Sol.-Terr. Phys., 66, pp. 493-506, doi:10.1016/j.jastp.2004.01.027, 2004.

Garcia, R. R. and Solomon, S.: The effect of breaking gravity waves on the dynamics and chemical composition of the mesosphere and lower thermosphere, J. Geophys. Res., 90, D2, pp. 3850-3868, 1985.

Gardner C. S., Zhao, Y., and Liu, A. Z.: Atmospheric stability and gravity waves dissipation in the mesopause region, J. Atmos. Sol.-Terr. Phy., 64, 923-929, 2002.

Gavrilov, N. M., Riggin, D. M., and Fritts, D. C.: Interannual variations of the mean wind and gravity wave variances in the middle atmosphere over Hawaii, J. Atmos. Sol.-Terr. Phy., Vol. 66, Issues 6-9, pp. 637-645, doi:10.1016/j.jastp.2004.01.015, 2004.

Atmospheric
Measurement
Techniques
Discussions

Hannawald P., Schmidt, C., Wüst , S., and Bittner, M.: A fast SWIR imager for observations of transient features in OH airglow, Atmos. Meas. Tech., 9 1461-1472, doi:10.5194/amt-9-1461-2016, 2016.

Hannawald, P., Schmidt, C., Sedlak, R., Wüst, S., and Bittner, M.: Seasonal and intra-diurnal variability of small-scale gravity waves in OH airglow at two Alpine stations, Atmos. Meas. Tech., 12,457–469, DOI: 10.5194/amt-12-457-2019, 2019.

Hibbins, R. E., Espy, P. J., Jarvis, M. J., Riggin, D. M., and Fritts, D. C.: A climatology of tides and gravity wave variance in the MLT above Rothera, Antarctica obtained by MF radar, J. Atmos. Sol.-Terr. Phy., Vol. 69, doi:10.1016/j.jastp.2006.10.009, pp. 578-588, 2007.

Hines C. O.: Internal atmospheric gravity waves at ionospheric heights, Canadian Journal of Physics, 38, No. 11, pp. 1441-1481, 1960.

Hines, C.O. and Tarasick, D.W.: On the detection and utilization of gravity waves in airglow studies, Planet. Space Sci., 35, 851–866, https://doi.org/10.1016/0032-0633(87)90063-8, 1987.

Hodges, R. R.: Eddy diffusion coefficients due to instabilities in internal gravity waves, J. Geophys. Res., 74, Issue 16, pp. 4087-4090, 1969.

Höppner, K. and Bittner, M.: Evidence for solar signals in the mesopause temperature variability?, J. Atmos. Sol.-Terr. Phy., 69, pp. 431-448, 2007.

Holton, J. R.: The influence of gravity wave breaking on the general circulation of the middle atmosphere, J. Atmos. Sci., 40, pp. 2497-2507, 1983.

Hoffmann P., Becker, E., Singer, W., and Placke, M.: Seasonal variation of mesospheric waves at northern middle and high latitudes, J. Atmos. Sol.-Terr. Phy., 72, pp. 1068-1079 , 2010.

Kramer, R., Wüst, S., Schmidt, C., and Bittner, M.: Gravity wave characteristics in the middle atmosphere during the CESAR campaign at Palma de Mallorca in 2011/2012: Impact of extratropical cyclones and cold fronts. J. Atmos. Sol.-Terr. Phys., 128, 8–23. DOI: 10.1016/j.jastp.2015.03.001, 2015.

Kramer, R., Wüst, S., and Bittner, M.: Investigation of gravity wave activity based on operational radiosonde data from 13 years (1997 – 2009): Climatology and possible induced variability, J. Atmos. Sol.-Terr. Phys., 140, pp.23-33, 2016.

Laštovička, J.: Forcing of the ionosphere by waves from below, J. Atmos. Sol.-Terr. Phys., 68, pp. 479-497, doi:10.1016/j.jastp.2005.01.018, 2006.

Leinert, C., Bowyer, S., Haikala, L. K., Hanner, M. S., Hauser, M. G., Levasseur-Regourd, A.-C., Mann, I., Mattila, K., Reach, W. T., Schlosser, W., Staude, H. J., Toller, G. N., Weiland, J. L., Weinberg, J. L., and Witt, A. N.: The 1997 reference of diffuse night sky brightness, Astron. Astrophys. Suppl. Ser., 127, 1-99, 1998.

Lindzen, R. S.: Turbulence and stress owing to gravity wave and tidal breakdown, J. Geophys. Res.: Oceans banner, 86, C10, pp. 9707-9714, 1981.

Lübken, F.-J. and von Zahn, U.: Thermal structure of the mesopause region at polar latitudes, JGR Atmospheres. Vol. 96, Issue D11, pp. 20841-20857, doi:10.1029/91JD02018, 1991.

Meinel, A. B.: OH Emission band in the spectrum of the night sky. Part II. The Astrophysical Journal, 111, p. 555, doi:10.1086/145296, 1950.

Melo, S., M. L., Lowe, R. P., and Russell, J. P.: Double-peaked hydroxyl airglow profiles observed from WINDII/UARS, J.
5   Geophys. Res.: Atmospheres banner, 105, D10, pp. 12397-12403, 2000.

Mulligan, F.J., Horgan, D.F., Galligan, J.G., Griffin, E.M.: Mesopause temperatures and integrated band brightnesses calculated from airglow OH emissions recorded at Maynooth (53.21N, 6.41W) during 1993. Journal of Atmospheric and Terrestrial Physics 57 (13), 1623–1637, 1995.

Noll, S., Kausch, W., Kimeswenger, S., Unterguggenberger, S., and Jones, A. M.: Comparison of VLT/X-shooter OH and
10   O2 rotational temperatures with consideration of TIMED/SABER emission and temperature profiles, Atmos. Chem. Phys., 16, pp. 5021-5042, doi:10.5194/acp-16-5021-2016, 2016.

Noll, S., Winkler, H., Goussev, O., and Proxauf, B.: OH level populations and accuracies of Einstein-A coefficients from hundreds of measured lines, Atmos. Chem. Phys. Discuss., https://doi.org/10.5194/acp-2019-1102, in review, 2019.

Ochadlick Jr., A. R., Kritikos, H. N., and Giegengack, R.: Variations in the period of the sunspot cycle, Geophys. Res. Let.,
15   Vol. 20, Issue 14, pp. 1471-1474, 1993.

Offermann, D., Gusev, O., Donner, M., Forbes, J. M., Hagan, M., Mlynczak, M. G., Oberheide, J., Preusse, P., Schmidt, H., and Russell III, J. M.: Relative intensities of middle atmosphere waves, J. Geophys. Res., 114, D06110, doi:10.1029/2008JD010662, 2009.

Pautet, P. D., Taylor, M. J., Pendleton, W. R., Zhao, Y., Yuan, T., Esplin, R., & McLain, D.: Advanced mesospheric
20   temperature mapper for high-latitude airglow studies, Appl. Opt., 53(26), 5934–5943, 2014.

Rauthe, M., Gerding, M., and Lübken, F.-J.: Seasonal changes in gravity wave activity measured by lidars at mid-latitudes, Atmos. Chem. Phys., 8., pp. 6775-6787, 2008.

Reisin, E.R., and Scheer, J.: Vertical propagation of gravity waves determined from zenith observations of airglow. Adv. Space Res., Vol. 27, 1743–1748, 2001.

25   Schmidt, C., Höppner, K., and Bittner, M.: A ground-based spectrometer equipped with an InGaAs array for routine observations of OH(3-1) rotational temperatures in the mesopause region, J. Atmos. Sol.-Terr. Phy., 102, pp. 125-139, 2013.

Schmidt, C., Dunker, T., Lichtenstern, S., Scheer, J., Wüst, S., Hoppe, U.-P., and Bittner, M.: Derivation of vertical wavelengths of gravity waves in the MLT-region from multispectral airglow observations, J. Atmos. Sol.-Terr.
30   Phy., 173, pp. 119-127, 2018.

Sedlak, R., Hannawald, P., Schmidt, C., Wüst, S., and Bittner, M.: High-resolution observations of small-scale gravity waves and turbulence features in the OH airglow layer, Atmos. Meas. Tech., 9, pp. 5955-5963, doi: 10.5194/amt-9-5955-2016, 2016.

She, C. Y., Yu, J. R., and Chen, H.: Observed thermal structure of a midlatitude mesopause, Geophys. Res. Let., Vol. 20, Issue 7, pp. 567-570, doi:10.1029/93GL00808, 1993.

Silber, I., Price, C., Schmidt, C., Wüst, S., Bittner, M., and Pecora, E.: First ground-based observations of mesopause temperatures above the Eastern-Mediterranean Part I: multi-day oscillations and tides, J. Atmos. Sol.-Terr. Phys.,
5   155, 95-103, 2017.

Simkhada, D.B., Snively, J.B., Taylor, M.J., and Franke, S.J.: Analysis and modeling of ducted and evanescent gravity waves observed in the Hawaiian airglow, Ann. Geophys. 27, 3213–3224, 2009.

Svenson, G. R. and Gardner, C. S.: Analytical models for the responses of the mesospheric OH* and Na layers to atmospheric gravity waves, J. Geophys. Res.: Atmospheres banner, 103, D6, pp. 6271-6294, 1998.

10   Taylor, M. J.: A review of advances in imaging techniques for measuring short period gravity waves in the mesosphere and lower thermosphere, Adv. Space Res., 19, pp. 667-676, 1997.

Ulrych, T. J. and Bishop, T. N.: Maximum entropy spectral analysis and autoregressive decomposition, Rev. Geophys. Space Phys., 13, 183-200, 1975.

von Savigny, C., Eichmann, K.-U., Llewellyn, E. J., Bovensmann, H., Burrows, J. P., Bittner, M., Höppner, K., Offermann,
15   D., Taylor, M. J., Zhao, Y., Steinbrecht, W., and Winkler, P.: First near-global retrievals of OH rotational temperatures from satellite-based Meinel band emission measurements, Geophys. Res. Lett., 31, L15111, 2004.

Wachter, P., Schmidt, C., Wüst, S., and Bittner, M.: Spatial gravity wave characteristics obtained from multiple OH(3-1) airglow temperature time series, J. Atmos. Sol.-Terr. Phy., 135, pp. 192-201, 2015.

Wüst, S., Wendt, V., Schmidt, C., Lichtenstern, S., Bittner, M., Yee, J.-H., Mlynczak, M. G., and Russell III, J. M.:
20   Derivation of gravity wave potential energy density from NDMC measurements, J. Atmos. Sol.-Terr. Phys., 138, 32–46, https://doi.org/10.1016/j.jastp.2015.12.003, 2016.

Wüst, S., Schmidt, C., Bittner, M., Silber, I., Price, C., Yee, J.-H., Mlynczak, M. G., and Russel III, J. M.: First ground-based observations of mesopause temperatures above the Eastern-Mediterranean Part II: OH*-climatology and gravity wave activity, J. Atmos. Sol.-Terr. Phys., 155, 104-111, 2017a.

25   Wüst, S., Bittner, M., Yee, J.-H., Mlynczak, M. G., and Russell III, J. M.: Variability of the Brunt–Väisälä frequency at the OH* layer height, Atmos. Meas. Tech., 10, 4895–4903, https://doi.org/10.5194/amt-10-4895-2017, 2017b.

Wüst, S., Offenwanger, T., Schmidt, C., Bittner, M., Jacobi, C., Yee, J.-H., Mlynczak, M. G., Russell III, J. M.: Derivation of gravity wave intrinsic parameters and vertical wavelength using a single scanning OH(3-1) airglow spectrometer. Atmos. Meas. Tech., 11, 2937–2947, DOI: 10.5194/amt-11-2937-2018, 2018.

30   Wüst, S., Schmidt, C., Hannawald, P., Bittner, M., Mlynczak, M. G., Russell III, J. M.: Observations of OH-airglow from ground, aircraft, and satellite: investigation of wave-like structures before a minor stratospheric warming. Atmos. Phys. Chem., 19, 6401–6418, DOI: 10.5194/acp-19-6401-2019, 2019.
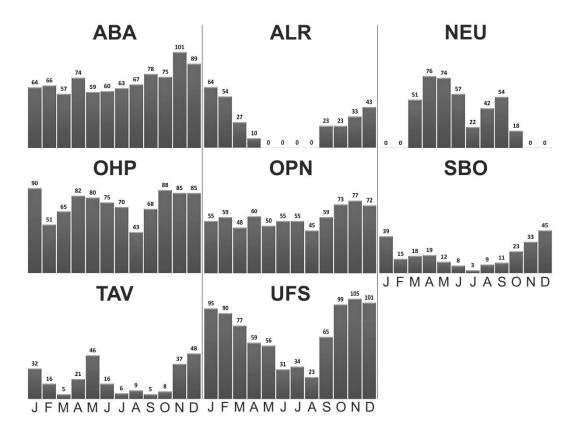
Figure 1. Monthly data coverage (the small numbers above each column indicate the number of nights) for the individual observation sites.
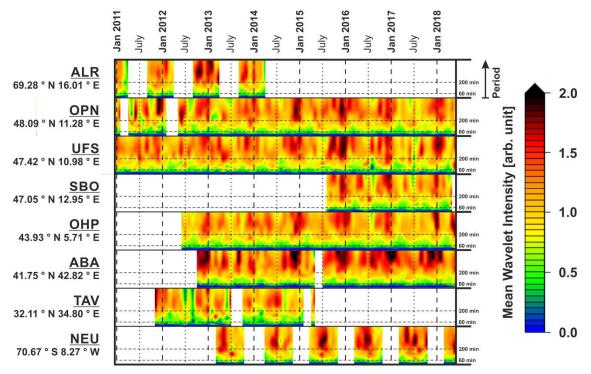
Figure 2. Long-term courses of monthly mean wavelet intensity in the period range between 6 and 480 min for different observation sites.
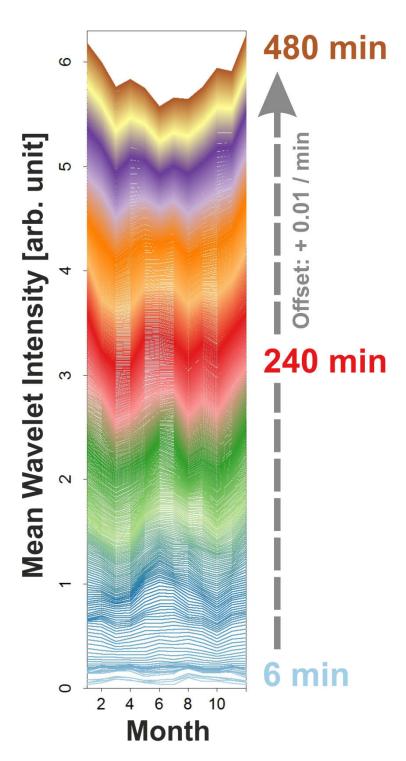
Atmospheric
Measurement
Techniques
Discussions

Figure 3. Monthly mean values of significant wavelet intensity averaged over all years at OPN. The cycles are separated by gravity wave period and have been coloured and provided with an offset of 0.01 per minute of wave period to make the gradual transition of annual behaviour with growing wave periods visible.
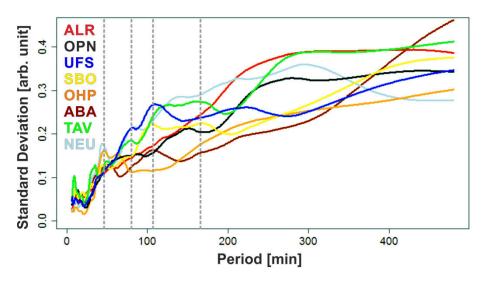
Atmospheric
Measurement
Techniques
Discussions

Figure 4. Standard deviation of the wavelet intensity for each period between 6 and 480 minutes and for all sites. The positions of local maxima around the periods 45min, 80min, 105min and 160min are marked by dashed grey lines.
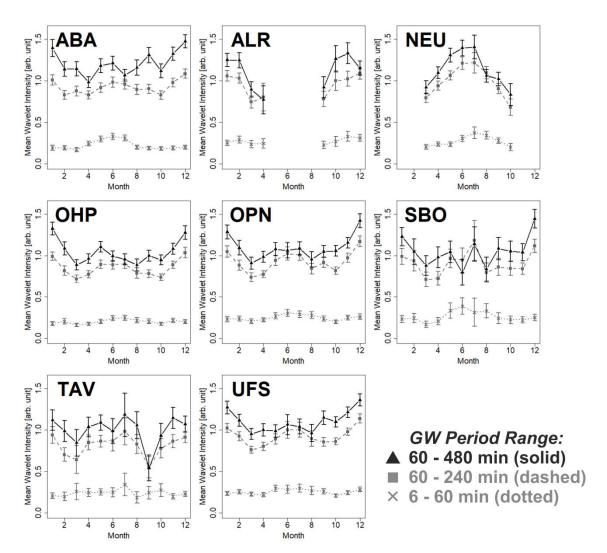
5

Figure 5. Monthly mean wavelet intensity averaged in the period ranges 6–60 min, 60–240 min, and 60–480 min. The error bars represent the standard error of the mean $\sigma/\sqrt{N}$ (with σ being the standard deviation of nocturnal values for each month and N the number of nocturnal values), which is larger than the uncertainty resulting from the individual error bars of the measurements, as it is calculated in our analysis.